AIAA Propulsion and Energy Forum
August 24-28, 2020, VIRTUAL EVENT
AIAA Propulsion and Energy 2020 Forum

10.2514/6.2020-3646

In Situ Measurement of Hall Thruster Cathode Fluctuations

Ethan T. Dale* and Benjamin A. Jorns†
University of Michigan, Ann Arbor, MI 48109

Measurements of Hall thruster cathode fluctuations are made *in situ* using an embedded pole cover probe. These fluctuations have been observed before but the connection between the measured modes remains elusive. Waves are measured with a high-speed camera, an embedded probe, and discharge current telemetry. These signals are compared in terms of frequencies and phases to establish properties of the observed modes. The results suggest that three modes are present: the breathing mode, a resonant global mode, and an azimuthal local cathode mode. The global and local modes are found to be distinct. The participation of the local mode in enhanced erosion is shown to be most likely minor. Further analysis suggests the frequency of the global mode is consistent with a 1:2:3 harmonic configuration.

I. Nomenclature

f_a	=	global frequency, Hz
f_b	=	breathing frequency, Hz
f_c	=	local frequency, Hz
m	=	mode number
m_e	=	electron mass, kg
m_i	=	ion mass, kg
n	=	plasma density, m^{-3}
T_e	=	electron temperature, eV
V_f	=	floating potential, V
$V_{f,p}$	=	floating pole potential, V
V_p	=	plasma potential, V
ω	=	angular frequency, rad/s

II. Introduction

Hall thrusters are an increasingly prevalent propulsion solution for near-Earth and deep space missions [1]. As with any in-space propulsion system, the stability and reliability of the technology is paramount. Unfortunately, Hall thrusters support a wide range of plasma instabilities [2], many of which remain poorly understood. Without the impact of these phenomena on thruster performance completely characterized, they pose a major liability for the practical application of Hall thrusters.

In particular, hollow cathodes – used as the electron source for Hall thrusters – can sustain many instabilities, often in unique ways when operated with a thruster versus alone. The existence of coherent, macroscopic azimuthal waves around centrally-mounted cathodes has previously been reported [3]. The influence of these waves on thruster behavior is still unclear. A major obstacle in understanding this instability is the inaccessibility of the near-cathode region to non-perturbative diagnostics.

The need is apparent, then, for dedicated experimental study of these waves using advanced diagnostic techniques. In this work, we first provide a description of these azimuthal waves. In Section IV we review the practical details of our experimenta to characterize these waves. After presenting the results, we discuss their implications for our understanding of the cathode instability in Section VI.

*Post-Doctoral Fellow, Department of Aerospace Engineering, 1919 Green Road, Ann Arbor, MI 48109, AIAA Student Member
†Assistant Professor, Department of Aerospace Engineering, 1320 Beal Avenue, Ann Arbor, MI 48109, AIAA Senior Member

III. Background

It has long been known that azimuthal oscillations can be supported in hollow cathode plumes [4–6]. The presence of a "cathode mode" in a Hall thruster has been identified using high-speed imaging by Jorns and Hofer [3]. In that study, the instability was characterized as a m=1 azimuthal mode with a frequency between the ion and electron gyrofrequencies and lower than either plasma frequency. Additionally, an apparently related spectral peak in the discharge current telemetry was detected, suggesting that the wave possibly transitions to a m=0 mode near the thruster channel.

Jorns and Hofer identify these waves as anti-drift waves [7], which are mediated by the diamagnetic drift and sustained by the phase offset of electrons due to collisional drag. Since then, it has been suggested that instabilities could contribute to pole cover erosion [8, 9], and that these anti-drift waves may play a role in anomalous cathode plume resistivity [10].

There remain several open questions about these waves. First, the relationship between these azimuthal waves to the global (m=0) mode observed in the discharge current signal is unclear. Second, the role these oscillations may play in the erosion of the pole cover has yet to be explored experimentally. In both cases, it is difficult to make non-perturbative measurements that yield enough information to make meaningful conclusions. In this work, we leverage measurements from four sources to attempt to overcome this issue: high-speed imaging, discharge current telemetry, a floating probe embedded in the inner pole cover, and a near-cathode Langmuir probe.

IV. Methodology

We now describe the practical details of the diagnostic tools we utilized, as well as a general description of the facility and thruster.

A. Facility and Thruster

The experiments were conducted at the University of Michigan in the Large Vacuum Test Facility (LVTF). The LVTF is a 6-m diameter, 9-m long stainless steel-clad vacuum chamber. Rough vacuum is attained with a series of four mechanical pumps and two Roots blowers, and high vacuum with thirteen two-stage cryogenic pumps and five cryosails. LVTF has a pumping speed of roughly 600 kL/s on xenon, reaching base pressures near <1 μTorr-N_2 and operating pressures ~2 μTorr-Xe. Figure 1a shows a photograph of the facility exterior.

The test device was a 9-kW magnetically-shielded Hall thruster developed by the Jet Propulsion Laboratory in collaboration with the Air Force Research Laboratory and the University of Michigan. Refs. 11 and 12 describe the design and performance of this thruster in detail. In the present work, it was operated at the nominal 300 V, 3 kW condition with a standard 7% cathode flow fraction. However, we also draw upon previous discharge current measurements from operation at 75% the nominal magnetic field strength at 3 kW, as well as operation at 300 V, 4.5 kW. Figure 1 shows a photograph of the thruster in operation.

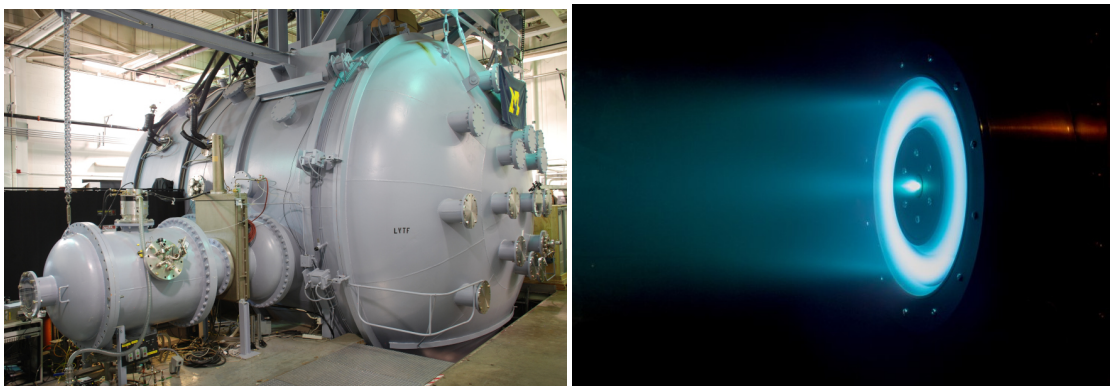

(a) **(b)**

Fig. 1 A photograph of the LVTF exterior (a) and the 9-kW thruster in operation (b).

B. Diagnostics

High-speed imaging was performed in this experiment to capture time-resolved light intensity in the vicinity of the cathode. We used a Photron FASTCAM SA5, imaging at 300 kfps with a resolution of 64x256. Figure 2 shows an annotated still; the entire cathode was captured as well as the 3 o'clock portion of the channel. The acquired video was analyzed following the principles described in Ref. 13.

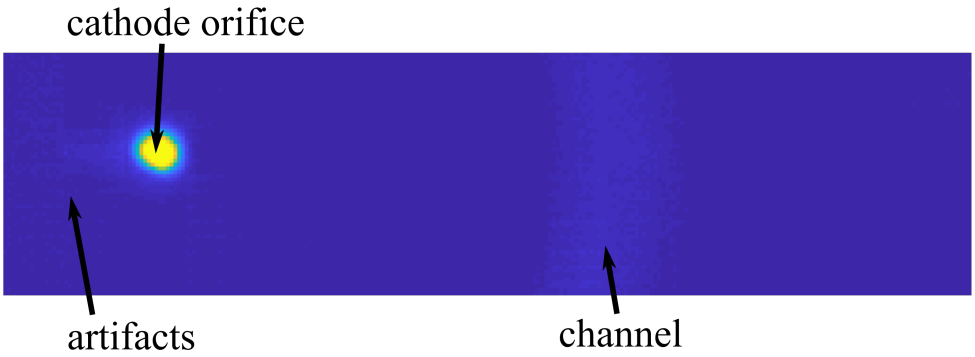

Fig. 2 A sample still showing the cathode orifice, the thruster channel, and sensor artifacts.

In a previous experiment, a Langmuir probe was used near the cathode of the thruster to establish time-averaged properties in the vicinity of the inner pole cover. Although the thruster was operating at 300 V, 4.5 kW, we believe this data is still meaningful for comparison with the present study. As described in Ref. 10, we used a cylindrical Langmuir probe with a collecting area ~ 1 mm^2. The data was acquiring by "pecking" the biased probe toward the thruster with a high-speed motion stage to minimize perturbation of the discharge.

A fine-wire probe was also embedded inside the inner pole cover to measure the near-cathode floating potential *in situ*. Figure 3 shows a schematic of the probe as well as a photograph of it in place. The exposed probe tip was located at the 5 o'clock position, approximately 40 mm from the cathode centerline. The wire diameter was 0.005" and the total interruption of the pole cover surface only 0.063" in diameter, minimizing its interaction with the local plasma. The probe wire was essentially flush with the surface of the pole cover. The probe potential was measured with a GW Instek GDS-1074B 70 MHz, 10^9 sample-per-second oscilloscope. The oscilloscope was synchronized with the FASTCAM so that any recorded traces were directly comparable with the high-speed video. The cathode discharge current was also recorded with the oscilloscope, measured with a Tektronix TCP303 active Hall current sensor.

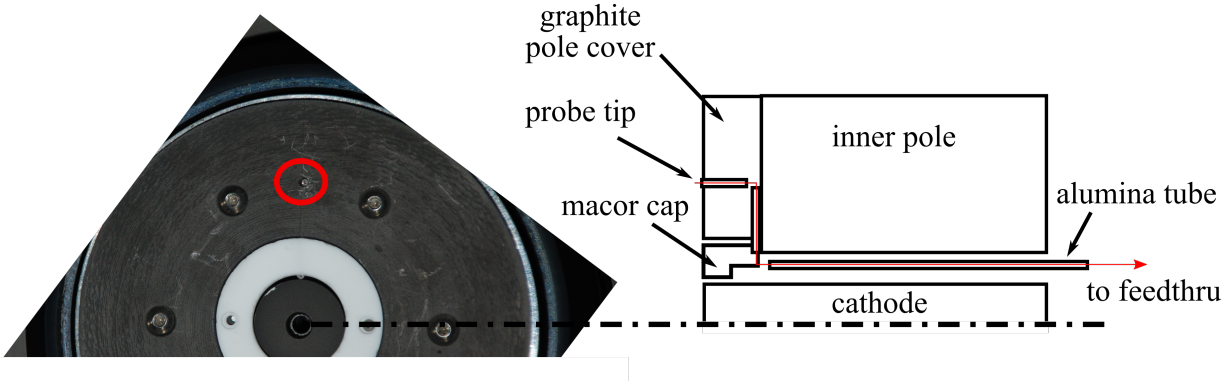

Fig. 3 A schematic of the embedded pole cover probe (right) and a scale photo of it implemented in the H9 with the probe location circled (left).

V. Results

We now present the results of this experiment. First we show a sample of the raw measurements made, including high-speed signals and time-averaged data. Following that, we present spectral data in the form of power spectra and maps of frequency and phase.

A. Raw Measurements

Figure 4 shows samples of raw traces of discharge current and floating pole potential. The discharge current has a peak-to-peak value of 4.76 A and a RMS of 0.56 A, which is typical for a nominal operating condition of this thruster. The floating potential had a mean of 1.00 V, a peak-to-peak of 4.80 V, and a RMS of 0.48 V. Morphologically, these two signals are fairly dissimilar but both appear rather incoherent.

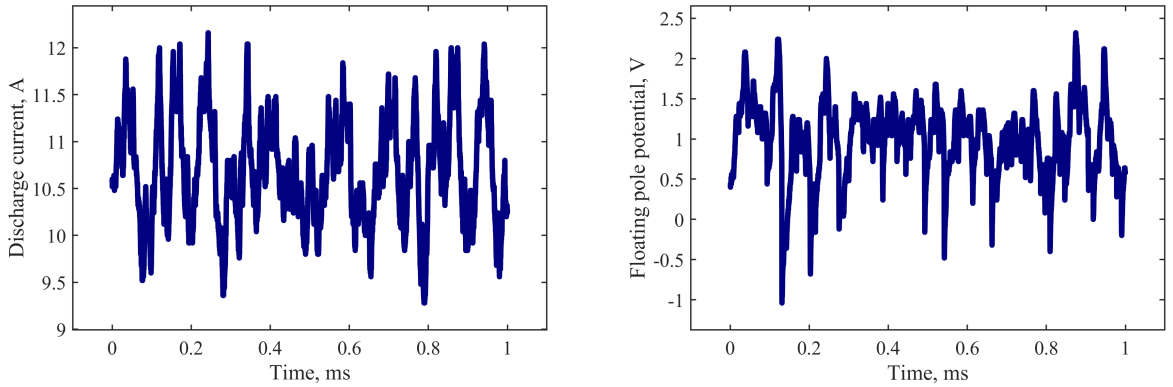

(a) **(b)**

Fig. 4 A sample of the raw discharge current trace (a) and the raw floating pole potential (b).

Figure 5 shows the time-averaged plasma potential V_p, density n, electron temperature T_e, and floating potential V_f as a function of axial distance from the pole cover as yielded by the near-cathode Langmuir probe. The distances are normalized by the channel length, L_{ch}. This data was taken roughly 25 mm from the cathode centerline, which is past the keeper face but not as far as the pole probe location. Observe that T_e, V_f, and V_p are nearly constant over the measured range, and n slightly increases farther from the pole cover. Nearest the pole cover, a fair estimate of the Debye length is therefore about 77 μm, and thus the sheath on the pole cover and floating probe are very thin.

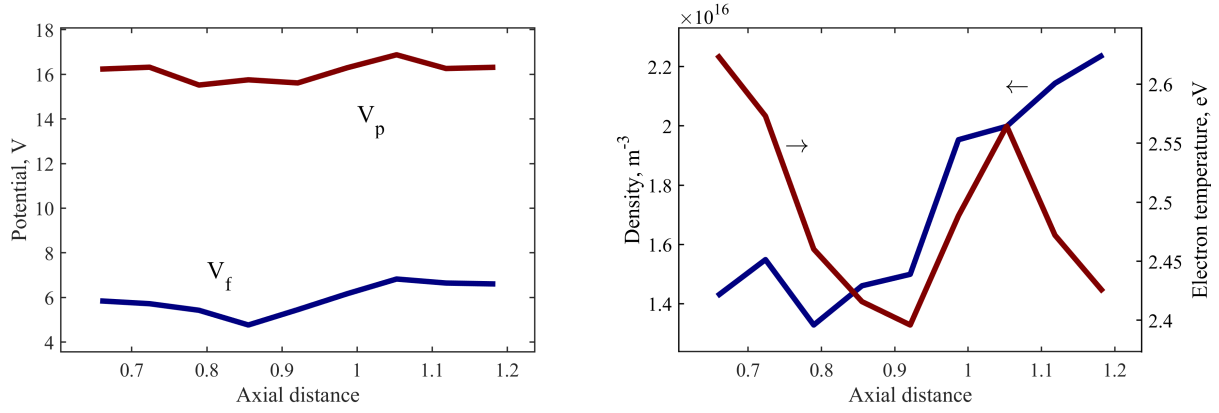

(a) **(b)**

Fig. 5 The near-cathode floating and plasma potentials (a), and the density and electron temperature (b).

Figure 6 shows a few sequential frames from the FASTCAM, demonstrating the significant variations in light emission from the cathode and channel over time. Note that even when the cathode plume is intense (68 ms), there are

considerable regions of dark (noise) pixels across the pole cover and beyond the channel.

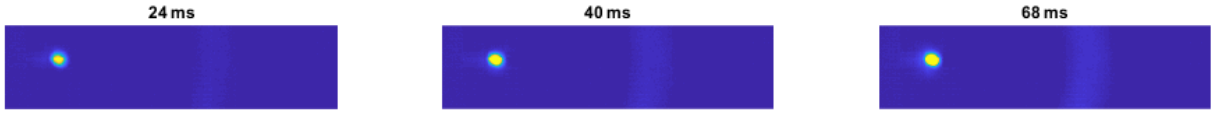

Fig. 6 Sequential frames from the high-speed video showing

B. Spectra

Figure 7 shows the power spectra of the discharge current I_d and floating pole potential $V_{f,p}$ signals, where the former has been vertically offset by 10^5 dB for comparison. These spectra were calculated using Bartlett's method to reduce noise. There appear to be three distinct modes and several harmonics in these spectra, including a broad low-frequency peak around 10-30 kHz, a defined peak $f_a \sim 60$ kHz, and another defined peak near $f_c \sim 80$ kHz. We can evaluate the phase offsets between signals and peaks, and we show this in Table 1, where θ_{I_d} and $\theta_{V_{f,p}}$ are the phases of the discharge current and floating pole potentials signals, respectively.

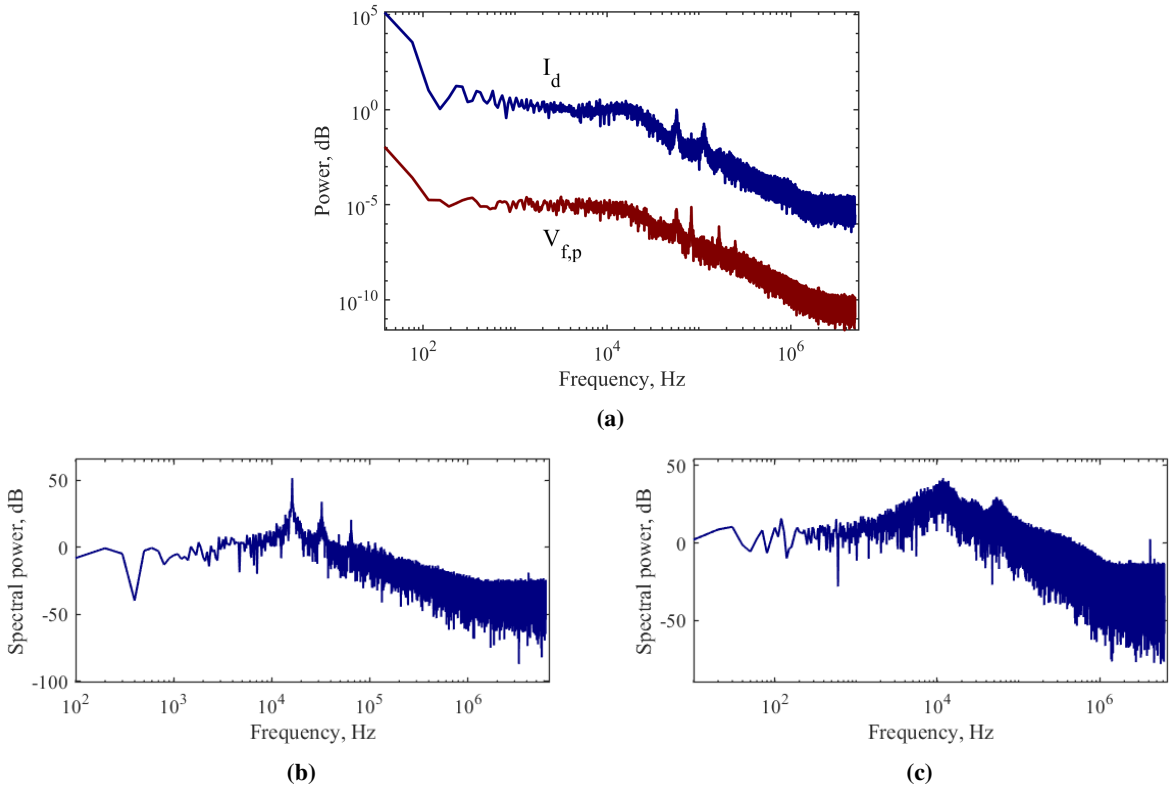

Fig. 7 Power spectra of the discharge current and floating pole potential signals from this experiment (a), and the discharge current at 3 kW and 75% magnetic field strength (b) and nominal 4.5 kW (c).

Figure 7 also shows for comparison the spectra at reduced magnetic field strength and at slightly higher power. In the former, the breathing mode is much more coherent and dominates the spectrum, with up to the eighth harmonic recognizable. At 4.5 kW, the breathing mode is again less coherent but appears to peak around 10 kHz. Here, there are recognizable peaks near 30 kHz and 50 kHz, but without an *in situ* measurement near the cathode, it is hard to determine if any of these correspond to the 80 kHz peak we see at the nominal 3 kW condition.

Figure 8 shows the frequency and phase of peak spectral power of the intensity of each non-noise pixel recorded by the high-speed camera. The former map indicates that most spectral content is near 80 kHz close to the cathode,

Table 1 Phase offsets between signals and peaks according to Fig. 7.

Signals	Offset
$\theta_{I_d}(f_a) - \theta_{I_d}(f_c)$	98°
$\theta_{V_{f,p}}(f_a) - \theta_{V_{f,p}}(f_c)$	-120°
$\theta_{I_d}(f_a) - \theta_{V_{f,p}}(f_a)$	87°
$\theta_{I_d}(f_c) - \theta_{V_{f,p}}(f_c)$	-131°

while most content is near 60 kHz close to the channel. Further, the phase map shows the characteristic "swirl" of an azimuthal mode near the cathode, while there is uniform phase in the channel, indicating a global mode.

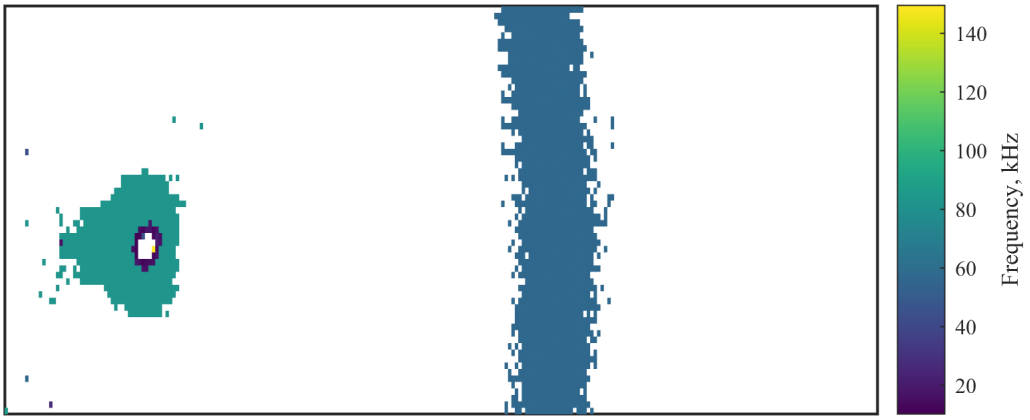

(a)

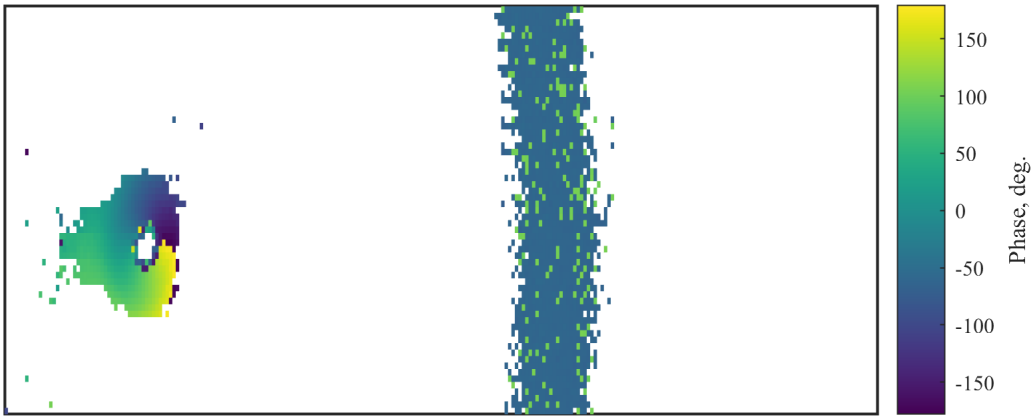

(b)

Fig. 8 A map of the frequency (a) and phase (b) of peak spectral power.

Figure 9 shows the entire power spectra at several locations over the inner pole cover from the intensities measured by the high-speed camera. Specifically, we show the signals within 1 mm of the cathode center, 5 mm away, 8 mm away, and 11 mm away, all in the 5 o'clock direction toward the floating probe. We additionally include the spectrum of the

intensity in the thruster channel at 3 o'clock (red). Like before, we offset each curve up by 10^4 dB for ease of comparison. As we saw in the I_d and $V_{f,p}$ spectra, there are two clear peaks near 60 and 80 kHz and broad low-frequency content around 10-30 kHz.

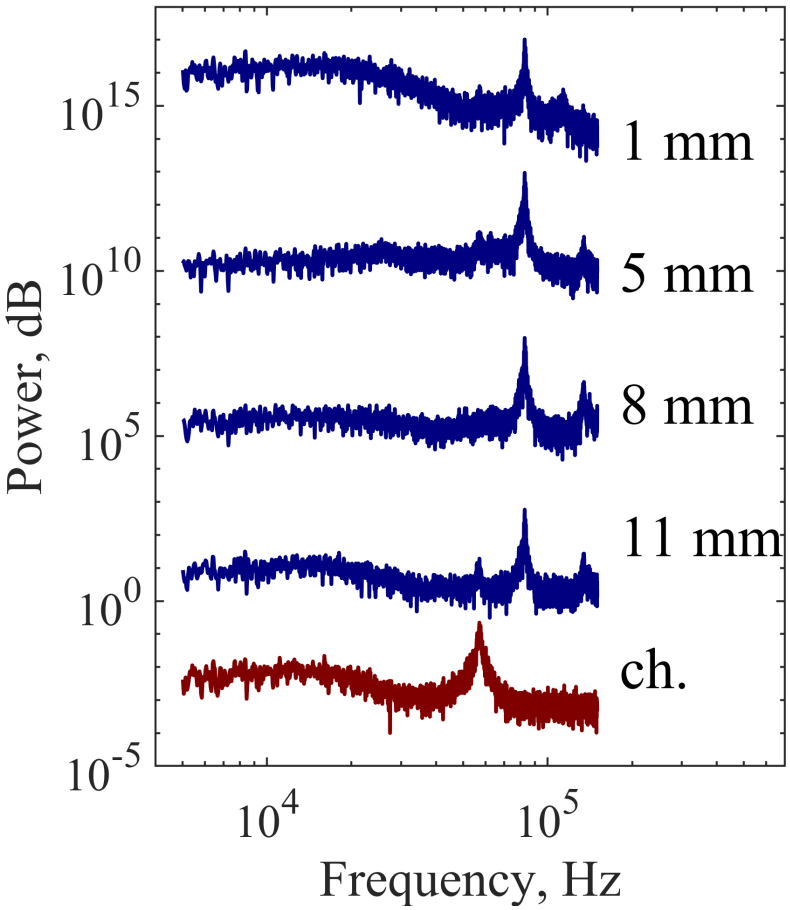

Fig. 9 Power spectra from the high-speed video at various distances from the cathode, as well as at the channel.

Based on Figs. 7 and 9, it is clear that three modes have been detected: the weak breathing mode at f_b = 10 to 30 kHz; a global mode at f_a = 57.1 kHz in I_d, $V_{f,p}$, and the high-speed video over the channel; and a local mode at f_c = 82.8 kHz in V_{f_p} and the high-speed video near the cathode. Unlike in the work of Jorns and Hofer [3], it appears here that the global mode is *not* in fact the breathing mode, a global instability typically observed in the discharge current signal at frequencies <30 kHz. All distinct peaks are roughly Lorentzian-shaped and often harmonics are present.

It is insightful to look at the phase of the local mode as a function of distance from the cathode, ranging from 2 to 10 mm away from it and normalized within 20° bins. Figure 10 shows this evolution. Although a large portion of the pole cover was too dark to yield meaningful FASTCAM data, even over this limited range there does appear to be consistent phasing around the cathode, as well as slightly increasing phase farther from cathode, which indicates that the wave is slightly tilted. The mean radial phase velocity implied by this data is about 3 km/s.

VI. Discussion

We now use these results to discussion the nature of the observed modes as well as these implications of the azimuthal mode on erosion of the pole cover.

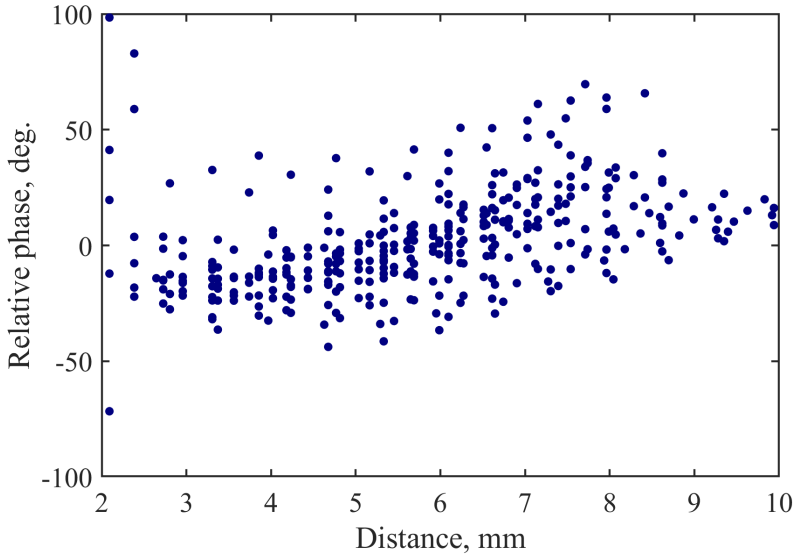

Fig. 10 Power spectra from the high-speed video at various distances from the cathode, as well as at the channel.

A. Mode Origins

There are several interesting aspects to the presented spectra that must be reviewed before drawing any conclusions about the relationship between the measured modes. First, the two modes have roughly equal strength at the location of the pole probe and are distinct. Second, the local mode can be slightly detected in the discharge current signal, and the global mode can be slightly detected in the FASTCAM signal over the pole cover. These observations suggest that the local mode does not transition into the global mode – they exist simultaneously as distinct peaks with no spectral content between – but that they are two modes that coexist. Naturally, based on the strength of the fluctuations, the local mode presumably originates at the cathode and the global mode in the channel. By examining the phase of the modes in I_d and $V_{f,p}$, we indeed find that the global mode is leading by about 118 to 123° in I_d and lagging by about -89 to -107° in $V_{f,p}$. This supports the notion that the global mode is propagating from the channel over the pole, and the local mode is propagating from the cathode to the channel.

We now must consider why the azimuthal local mode can be detected in I_d at all before finally questioning how the two modes are related in Section VI.C, now that we have established the modes are distinct. In Ref. 3, the global mode was ~9 times slower than the local mode. This suggests that the detection of the latter in I_d is unrelated to any interaction with the former, as the azimuthal wave completed several cycles during a single global period. One possibility is that azimuthal asymmetries in the thruster – geometry, gas distribution, temperature, etc. – modulate the local mode such that it is detected in I_d. Given that a study with a segmented anode on a similar thruster in Ref. 13 in fact found up to a 6.5% difference in current conducted between the electrodes of a twelve-segment anode, this seems quite likely.

B. Implications for Erosion

In Section III we noted that instabilities near the cathode were proposed as a possible mechanism for enhancing erosion of the inner pole, which has been observed since the early characterization of magnetically-shielded Hall thrusters [14]. Armed with our measurement of $V_{f,p}$, we can attempt to shed some light on this possibility.

We start by acknowledging that the floating potential does not provide a very direct evaluation of erosion. Instead, it is a function of T_e and V_p:

$$V_f = V_p - T_e \ln\sqrt{\frac{m_i}{2\pi m_e}} \quad . \tag{1}$$

But even given this limitation, certain observations can be made based on our experiment. First, $V_{f,p}$ only fluctuates by at most 4.8 V, which implies either the plasma potential near the pole cover is fluctuating only very little, or it is changing significantly and T_e is also strongly oscillating out of phase. As we shown in Fig. 11, light intensity is roughly out of phase with $V_{f,p}$, which implies that n and T_e may also be out of phase with $V_{f,p}$. But fluctuations in T_e of only

0.91 eV are required to explain the floating potential trends, which seems reasonable given the average value of about 2.6 eV shown in Fig. 5. It seems implausible, then, that the plasma potential is changing significantly, and thus it is unlikely that ion energies are particularly enhanced by the azimuthal mode.

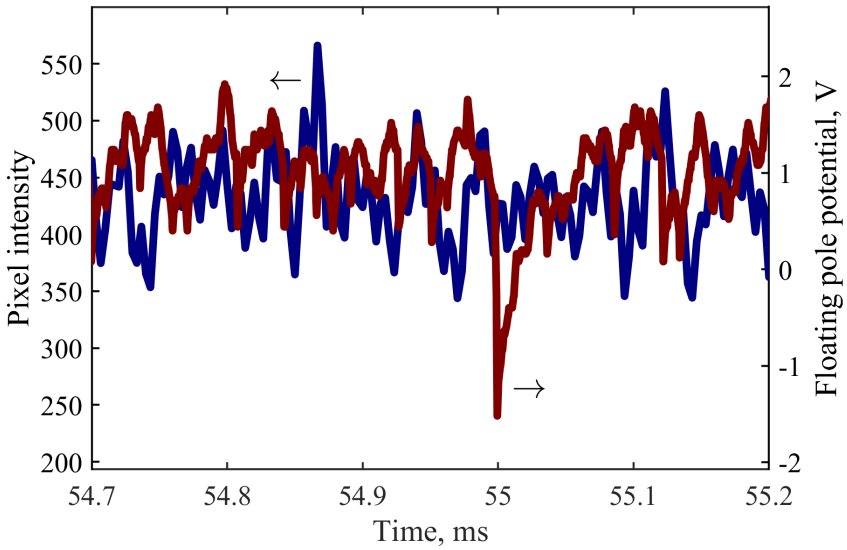

Fig. 11 A sample of the time-resolved pixel intensity 5 mm from the cathode centerline, and a sample of the floating pole potential signal.

Additionally, we can judge the symmetry of the $V_{f,p}$ fluctuations by comparing the range below and above the mean value. Doing this, we find this symmetry to be about 1.8, meaning that there is considerably greater variation below the mean than above it. This implies that $V_{f,p}$ does not contain sharp spikes above its mean value, and so even if erosion of the inner polar is highly nonlinear with V_p, it is unlikely that these floating potential measurements are consistent with enhanced erosion.

C. Global Mode

Finally, we should postulate on the nature of the global mode. As we discussed previously, the low-frequency hill observed in most spectra is most likely related to the breathing mode. This instability is seen ubiquitously in Hall thrusters and is characterized by discharge current oscillations ~10 kHz. The azimuthal mode at 83 kHz can also be easily identified as the cathode anti-drift wave. However, there is no obvious candidate for an instability that describes the 57 kHz global mode.

If we remove the log-linear attenuation above ~18 kHz (seen in Fig. 7, as shown in Fig. 12, we can clearly delineate the center of this hill as about 28-30 kHz. Interestingly, the global mode and local mode are the second and third harmonic of this fundamental breathing frequency.

The presence of harmonics in a power spectrum is not always indicative of the existence of a separate physical mode – any non-sinusoidal wave will have harmonics in its Fourier transform. However, our FASTCAM measurements verify that the 83 kHz third harmonic is indeed a real phenomenon unrelated to the breathing mode. On the other hand, from the data we have gathered we cannot definitively state that the global mode is a physical mode separate from the breathing mode rather than just a harmonic. However, the sharpness of the global mode peak in all spectra is unusual considering how broad the breathing mode hill appears. It seems more likely, then, that the global mode is not just a harmonic but is a separate, physical mode somehow related to the breathing mode. But like in the case of the resonance that exists between the breathing mode and azimuthal mode, it is likely that the global mode has a similar origin to the breathing mode and is simply coerced to the second harmonic frequency.

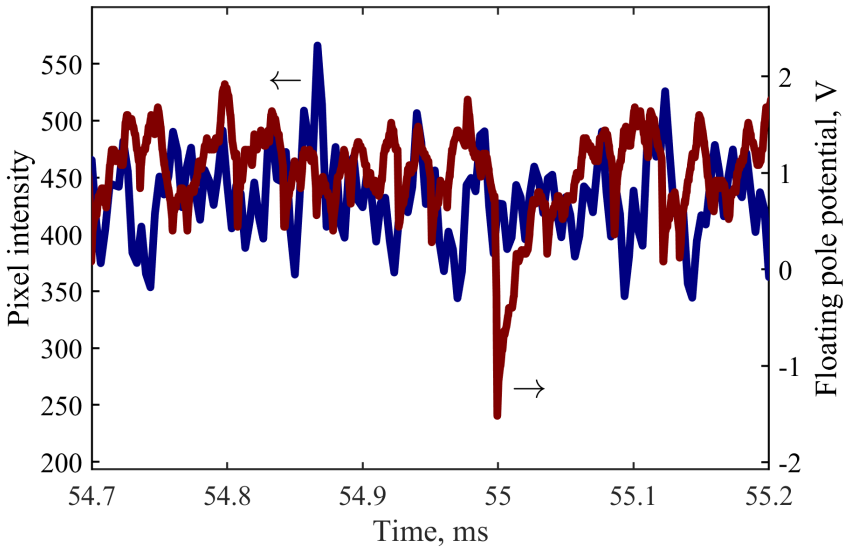

Fig. 12 The discharge current spectrum with high-frequency attenuation removed to highlight the center of the low-frequency breathing mode hill.

VII. Conclusions

In this work we have measured cathode fluctuations in a magnetically-shielded Hall thruster using several sources: a high-speed camera, discharge current telemetry, and a floating probe embedded in the inner pole cover. We additionally had access to near-cathode time-averaged measurements for the sake of characterizing the plasma environment over the pole cover.

We examined these signals in terms of frequency and phase at various spectral peaks. In general, we observed a broad low-frequency hill associated with the breathing mode, a defined global peak at 57 kHz, and a defined local peak at 83 kHz. The coexistence of the global and local modes in certain locations suggests that these are separate modes, not manifestations of the same oscillation. We additionally argue that azimuthal asymmetries are a reasonable explanation for the detection of the local mode in the discharge current signal. Based on the magnitude of symmetry of floating potential measurements, we conclude that the azimuthal mode does not seem to play a large role in enhanced inner pole erosion. Finally, we observe that all detected modes are harmonics, and thus we suggest the global mode is a resonant offshoot of the breathing mode.

References

[1] Oh, D. Y., Snyder, J. S., Goebel, D. M., Hofer, R. R., and Randolph, T. M., "Solar Electric Propulsion for Discovery-Class Missions," *Journal of Spacecraft and Rockets*, Vol. 51, No. 6, 2014, pp. 1822–1835. https://doi.org/10.2514/1.A32889, URL https://doi.org/10.2514/1.A32889.

[2] Choueiri, E. Y., "Plasma oscillations in Hall thrusters," *Physics of Plasmas (1994-present)*, Vol. 8, No. 4, 2001, pp. 1411–1426. https://doi.org/10.1063/1.1354644, URL http://scitation.aip.org/content/aip/journal/pop/8/4/10.1063/1.1354644.

[3] Jorns, B. A., and Hofer, R. R., "Plasma oscillations in a 6-kW magnetically shielded Hall thruster," *Physics of Plasmas (1994-present)*, Vol. 21, No. 5, 2014. https://doi.org/10.1063/1.4879819, URL http://scitation.aip.org/content/aip/journal/pop/21/5/10.1063/1.4879819.

[4] Morse, D. L., "Plasma Rotation in a Hollow-Cathode Discharge," *The Physics of Fluids*, Vol. 8, No. 3, 1965, pp. 516–521. https://doi.org/10.1063/1.1761253, URL http://aip.scitation.org/doi/10.1063/1.1761253, publisher: American Institute of Physics.

[5] Pots, B. F. M., Coumans, J. J. H., and Schram, D. C., "Collective scattering of CO2-laser light from ion-acoustic turbulence," *The Physics of Fluids*, Vol. 24, No. 3, 1981, pp. 517–527. https://doi.org/10.1063/1.863400, URL http://aip.scitation.org/doi/10.1063/1.863400, publisher: American Institute of Physics.

[6] Galansky, V. L., Gruzdev, V. A., Osipov, I. V., and Rempe, N. G., "Physical processes in plasma electron emitters based on a hollow-cathode reflected discharge," *Journal of Physics D: Applied Physics*, Vol. 27, No. 5, 1994, pp. 953–961. https://doi.org/10.1088/0022-3727/27/5/012, URL https://doi.org/10.1088%2F0022-3727%2F27%2F5%2F012, publisher: IOP Publishing.

[7] Sakawa, Y., Joshi, C., Kaw, P. K., Chen, F. F., and Jain, V. K., "Excitation of the modified Simon–Hoh instability in an electron beam produced plasma," *Physics of Fluids B: Plasma Physics*, Vol. 5, No. 6, 1993, pp. 1681–1694. https://doi.org/10.1063/1.860803, URL https://aip.scitation.org/doi/10.1063/1.860803.

[8] Polk, J. E., Lobbia, R., Barriault, A., Guerrero, P., Mikellides, I., and Lopez Ortega, A., "Inner Front Pole Cover Erosion in the 12.5 kW HERMeS Hall Thruster Over a Range of Operating Conditions," *35th International Electric Propulsion Conference*, Atlanta, GA, 2017.

[9] Lopez Ortega, A., and Mikellides, I., "Investigations of Pole Erosion Mechanisms in the 12.5 kW HERMeS Hall Thruster with the Hall2De Code," *35th International Electric Propulsion Conference*, Atlanta, GA, 2018. https://doi.org/10.2514/6.2018-4647.

[10] Jorns, B. A., Cusson, S. E., Brown, Z., and Dale, E., "Non-classical electron transport in the cathode plume of a Hall effect thruster," *Physics of Plasmas*, Vol. 27, No. 2, 2020, p. 022311. https://doi.org/10.1063/1.5130680, URL https://aip.scitation.org/doi/10.1063/1.5130680, publisher: American Institute of Physics.

[11] Hofer, R., Cusson, S., Lobbia, R., and Gallimore, A., "The H9 Magnetically Shielded Hall Thruster," *35th International Electric Propulsion Conference*, Vol. IEPC- 2017- 232, 2017.

[12] Cusson, S., Hofer, R., Lobbia, R., Jorns, B., and Gallimore, A., "Performance of the H9 Magnetically Shielded Hall Thrusters," *35th International Electric Propulsion Conference*, Vol. IEPC-2017-239, 2017.

[13] McDonald, M. S., Bellant, C. K., Pierre, B. A. S., and Gallimore, A. D., "Measurement of cross-field electron current in a Hall thruster due to rotating spoke instabilities," *47th AIAA/ASME/SAE/ASEE Joint Propulsion Conference & Exhibit*, American Institute of Aeronautics and Astronautics, San Diego, CA, 2011. URL http://arc.aiaa.org/doi/pdf/10.2514/6.2011-5810.

[14] Sekerak, M. J., Hofer, R. R., Polk, J. E., Jorns, B. A., and Mikellides, I. G., "Wear Testing of a Magnetically Shielded Hall Thruster at 2000 s Specific Impulse," *Joint Conference of 30 th International Symposium on Space Technology and Science, 34 th International Electric Propulsion Conference and 6 th Nano-satellite Symposium*, Kobe, Japan, 2015. URL https://pdfs.semanticscholar.org/f84f/819fcacdef84730ca3e4b8311eafaeaf1eba.pdf.